Research Paper
Journal of Aerospace System Engineering
Vol.15, No.6, pp.1-9 (2021)
EISSN 2508-7150
http://dx.doi.org/10.20910/JASE.2021.15.6.1

Design and Performance Evaluation of Extension-Type Actuators with a Displacement Amplification Mechanism Based on Chevron Beam

Yehrin Jo[1], Euntaek Lee[2] and Yongdae Kim[1,†]
[1]Kyungil University
[2]Kumoh National Institute of Technology

Abstract

In this study, a new design of an extension-type actuator (ExACT) is proposed based on a chevron structure with displacement amplification mechanisms by local heating. ExACT comprises diamond-shaped displacement amplification structures (DASs) containing axially oriented V-shaped chevron beams, a support bar that restricts lateral heat deformation, and a loading slot for thin-film heaters. On heating the thin film heater, the diamond-shaped DASs undergo thermal expansion. However, lateral expansion is restricted by the support bar, leading to displacement amplification in the axial direction. The performance parameters of ExACT such as temperature distribution and extended displacement is calculated using thermo-mechanical analysis methods with the finite element method (FEM) tool. Subsequently, the ExACTs are fabricated using a polymer-based 3D printer capable of reproducing complex structures, and the performance of ExACTs is evaluated under various temperature conditions. Finally, the performance evaluation results were compared with those of the FEM analysis.

Key Words : 3D printing, Chevron actuator, Displacement amplification mechanism, Linear actuator

1. Introduction

An actuator is a mechanical device that converts input energy, which may be electric, hydraulic, or pneumatic into mechanical energy to generate motion such as linear or rotational motion. The primary types of actuators in use are electric actuators using motors or hydraulic/pneumatic actuators using high-pressure fluid. However, both these actuator types have certain drawbacks. Despite high rotational speeds, motors have small operating torques, necessitating a reduction mechanism to amplify the torque required to adapt it for use as an electric actuator. This increases the design complexity and the size and weight of the actuator. Hydraulic/pneumatic actuators are larger and heavier than electric actuators owing to the storage tank for energy storage in addition to a compressor unit, valves, sensors, and pipes. Therefore, despite applicability to large-sized systems, these types of actuators are infeasible in small-sized systems such as microrobots or micro-aircrafts.

Therefore, for the application of the actuators in microscale mechanical systems, new types of actuators capable of directly converting electrical energy into mechanical energy without a motor or hydraulic/pneumatic pressure are actively being researched [1]–[5]. These actuators have the advantages of a simple structure, limited weight, and reduced size and integration.

In this study, a high-displacement artificial-muscle type electrothermal actuator was developed. In electrothermal actuators, thermal energy generated by power supply is converted into mechanical energy, and the representative types include hot-and-cold-arm [6], chevron [7]–[9], and bimorph[10]–[12] actuators. In this study, a small electrothermal actuator developed was based on the chevron structure.

The chevron actuators operate based on the total thermal expansion consisting of a single material instead of using the differences in the coefficient of thermal expansion of the different structural materials. A typical chevron actuator has a V-shaped beam structure with limited lateral heat deformation, leading to displacement amplification in the axial direction. Despite a low driving voltage it is capable of generating large forces [5]. In particular, with their simple structure and large actuation displacement, chevron actuators are commonly used as miniaturized micro-actuators. Since the early reports of the chevron actuators by R. Cragun [13], L. Que [14], and M.J. Sinclair [15], various types of chevron actuators have been actively researched [5].

In this study, a design of an extension type actuator (ExACT)

Received: Jan. 11, 2021 Revised: Jul. 15, 2021 Accepted: Jul. 20, 2021
† Corresponding Author
Tel: +82-53-600-5350, E-mail: ydkim@kiu.kr

characterized by displacement amplification in axial direction under local heating is proposed. In particular, the proposed ExACT comprises the diamond-shaped displacement amplification mechanism in which V-shaped chevron beams, which have been extensively investigated in previous studies, are arranged in the axial direction. This arrangement functions as a linear actuator with a significantly larger actuation displacement than that induced by simple thermal expansion. The ExACT has a complex shape with 10 unit actuators comprising a displacement amplification structure (DAS) made of the same material and a support bar connected in series.

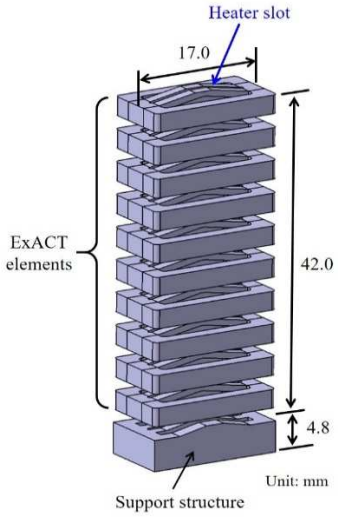

(a)

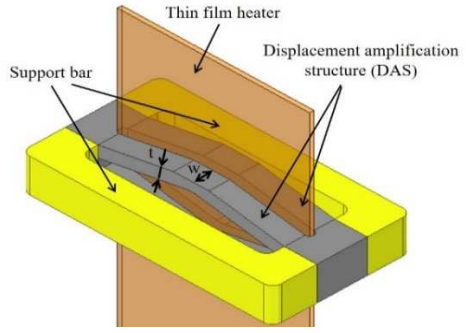

(b)

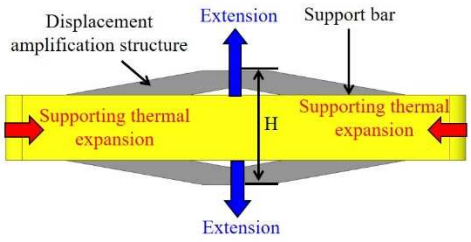

(c)

Fig. 1 Schematic of extension-type actuator (ExACT)

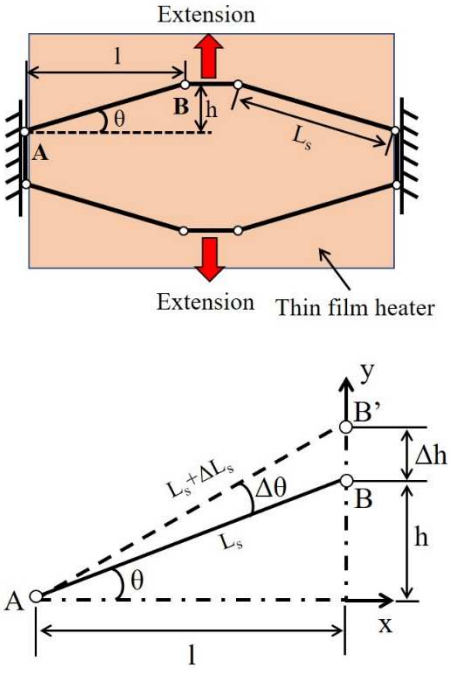

Fig. 2 Kinematic model of ExACT

By applying electricity to a thin film heater inserted into the inner slot, the whole structure is connected in series and heat is applied to the actuator, leading to extension in the axial direction. In this study, performance metrics of the developed ExACT such as actuation displacement was predicted through thermo-mechanical analysis using finite element method (FEM)-based simulation software. Also, ExACT was fabricated using a 3D printer of the Selective Laser Sintering (SLS) method and performance evaluation of the ExACT was performed.

Consequently, the performance measured in the experiment with the fabricated ExACT and that calculated using the FEM analysis software were compared.

2. Design of ExACT

The proposed ExACT has a structure in which 10 unit actuators are connected in series as illustrated in Fig. 1 (a). Slots are present, into which one or two sheets of thin film heaters can be inserted. The total length of ExACT is approximately 42.0 mm, the width is 17.0 mm, and the thickness is 9.4 mm.

The geometry and the conceptual diagram of the operation of individual actuators are illustrated in Figs. 1 (b) and (c), respectively. The unit actuator consists of a DAS, support bar, and thin film heater. The thin film heater is inserted through the center of the actuator as shown in Fig. 1 (b). The operating mechanism of ExACT is shown in Fig. 1 (c). When heated, the diamond-shaped DAS located inside undergoes thermal

Table 1 Properties of Duraform PA [16]

Density (ρ)		1140 kg/m^3
Specific heat (C_p)		1500 J/kg·K
Thermal conductivity (k)		0.243 W/m·K
Coefficient of thermal expansion (α)	22-50°C	6.67×10^{-5} /°C
	above 50°C	14.9×10^{-5} /°C

expansion in both the lateral as well as axial direction. The design ensures a delay in heat transfer from the thin film heater to the support bar by placing it outside the structure. Therefore, the support bar has a relatively low temperature compared to the DAS placed inside and exhibits limited thermal expansion, thereby restricting the thermal expansion of the DAS in the lateral direction.

A simplified schematic of the geometry of DAS is presented in Fig. 2 (a). When DAS is heated, its length increases. However, since the lateral displacement is restricted by the support bar, the length varies only in the axial direction. Therefore, when elastic deformation is neglected, it can be assumed that AB in DAS rotates counterclockwise with reference to point A. At this time, point B moves to B', and h, the axial length of DAS increases by Δh as shown in Eq. 1.

$$\Delta h = \sqrt{(L_s + \Delta L_s)^2 - l^2} - h . \quad (1)$$

In Eq. 1, ΔL_s denotes the extended length of DAS by thermal expansion, and it can be calculated using Eq. 2, as shown below.

$$\Delta L_s = L_s \cdot \alpha \cdot \Delta T . \quad (2)$$

In Eq. 2, α and ΔT indicate the coefficient of thermal expansion and temperature variation of DAS, respectively. If Eq. 1 is rearranged briefly using Eq. 2, Eq. 3 can be obtained as follows

$$\frac{\Delta h}{h} = \frac{1}{\sin\theta}\sqrt{(1+\alpha\Delta T)^2 - \cos^2\theta} - 1 . \quad (3)$$

In order to examine the effectiveness of the diamond-shaped DAS, the axial length of thermal expansion of ExACT was compared with that of thermal expansion of a simple rectangular bar of length h. The length of thermal expansion of the rectangular bar of length h can be calculated using Eq. 4, as shown below.

$$\Delta h_{bar} = h \cdot \alpha \cdot \Delta T . \quad (4)$$

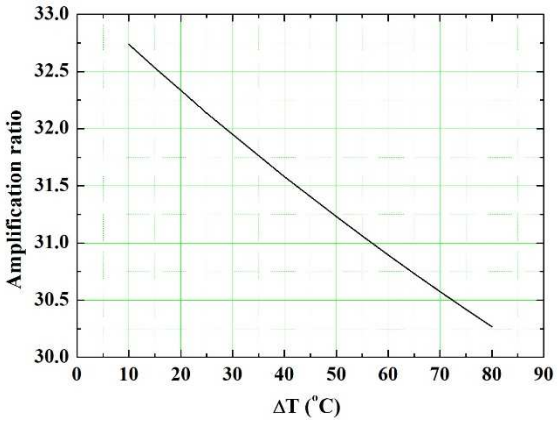

Fig. 3 Amplification ratio as a function of temperature variation

Table 2 Geometries of the ExACT

θ	H (mm)	h (mm)	w (mm)	t (mm)	l (mm)
10	4.20	0.76	1.4	0.80	4.38

Figure 3 presents a graph comparing the lengths of thermal expansion. The amplification ratio representing the ratio of the length of thermal expansion of ExACT to that of the rectangular bar is calculated as $\Delta h_{ExACT}/\Delta h_{bar}$. In Fig. 3, it can be seen that the length of thermal expansion of ExACT is amplified by more than 30 times that of a simple bar of length h.

Since the length of the thin film heater used in this study was 54 mm and the length of the part where the double heaters are formed was about 42 mm, the geometry of ExACT was designed as shown in Table 1 to ensure that each of the 10 unit actuators had a length (H) within 4.2 mm.

3. FEM analysis

To investigate the temperature distribution and thermal expansion characteristics of the actuator with the heating of the thin film heater, numerical analysis was performed using the FEM analysis software. Table 2 shows the material properties of Duraform PA (Nylon 6) used to fabricate the actuator. It was assumed that the heat loss on the actuator surface is caused by natural convection and mirrors the heat transfer in a flat horizontal plate with a hot upper surface. Since the convective heat transfer coefficient of natural convection is determined by the temperature of the heater, the Nusselt number as shown below was used to calculate the coefficient [17].

$$Nu = 0.54 Ra^{1/4} \quad (5)$$

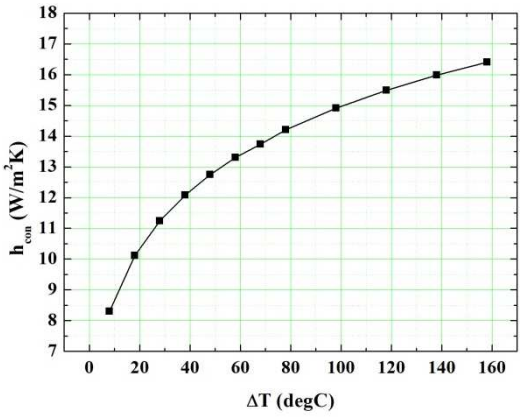

Fig. 4 Convective heat transfer coefficient as a function of ΔT

where *Ra* denotes Rayleigh number, and is expressed, as shown below [17].

$$Ra = Gr \cdot Pr = \frac{g\beta(T_s - T_\infty)L_c^3}{\nu^2} = \frac{g\beta(T_s - T_\infty)L_c^2}{\nu\eta}, \quad (6)$$

where *Gr* denotes Grashof number, *Pr* denotes Prandtl number, g is the gravitational acceleration, β is the coefficient of volume expansion, T_s is the temperature on the actuator surface, T_∞ is ambient temperature, L_c is characteristic length, ν is kinematic viscosity, and η is thermal diffusivity. For all values of physical properties, the temperature on the actuator surface and the value of film temperature condition of ambient temperature. Also, assuming air as an ideal gas, for the coefficient of volume expansion, the inverse of the absolute temperature of air was used. The convective heat transfer coefficient h_{con} can be calculated using Eq. 7.

$$h_{con} = \frac{Nu \cdot k_{air}}{L_c}, \quad (7)$$

where k_{air} represents the heat transfer coefficient of air. Figure 4 shows the convective heat transfer coefficient calculated using Eq. 7. At low surface temperature, its difference from ambient temperature is small, exhibiting small values of convective heat transfer coefficient. Conversely, at high surface temperature, the temperature difference increases, exhibiting large values of convective heat transfer coefficient. Approximately 29,000 tetrahedral and hexahedral elements were used for numerical analysis. To ensure structural boundary conditions, a fixed support condition applied to the bottom of the support structure prevented displacement, whereas other surfaces were permitted to exhibit unconstrained displacement For thermal boundary conditions, the heat flux on the heater area generated with respect to the set voltage was transferred to the chevron structure, and for all

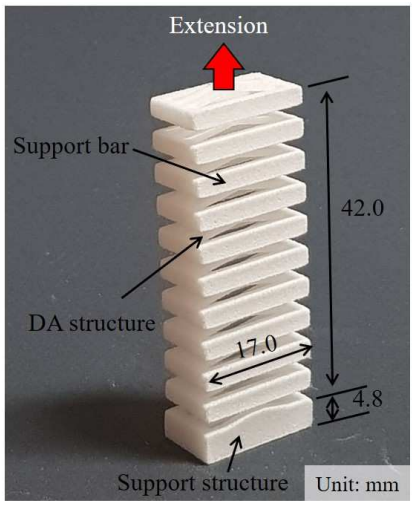

Fig. 5 Fabricated ExACT with 3D printer

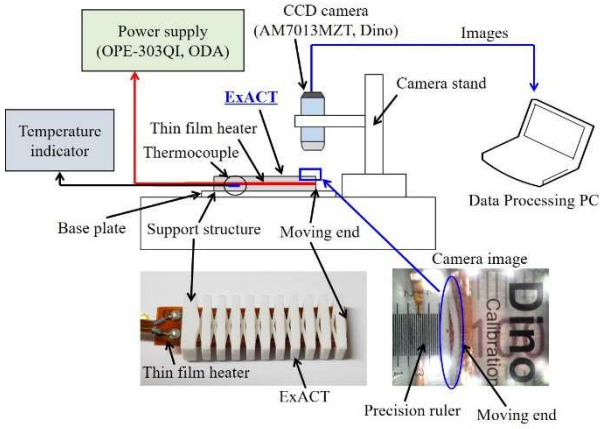

Fig. 6 Experimental setup for performance evaluation of ExACT

the other surfaces, natural convection conditions according to the convective heat transfer coefficient were applied. An initial temperature condition of 22°C was adopted during the experiment. By entering the values of the convective heat transfer coefficient in Fig. 4 into ANSYS, the temperature distribution inside the actuator and actuation displacement were calculated as a function of time up to 100 seconds.

4. Fabrication and Performance Evaluation

The fabrication of ExACT with general machining is difficult due to its highly complex structure with 10 unit actuators consisting of a support bar and DAS connected in series. Therefore, 3D printer (ProX 500 Plus, 3D SYSTEMS Inc.) using the selective laser sintering (SLS) method that facilitates implementation of complex structures was used for the fabrication of ExACT, and polyamide (Duraform PA,

Nylon 6)

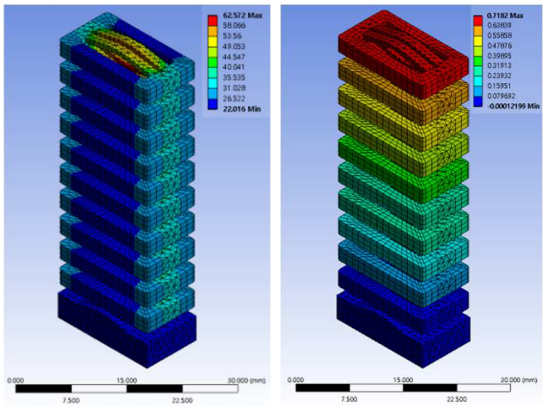

(a) (b)

Fig. 7 FEM analysis results: (a) temperature distribution and (b) retraction displacement at 4V

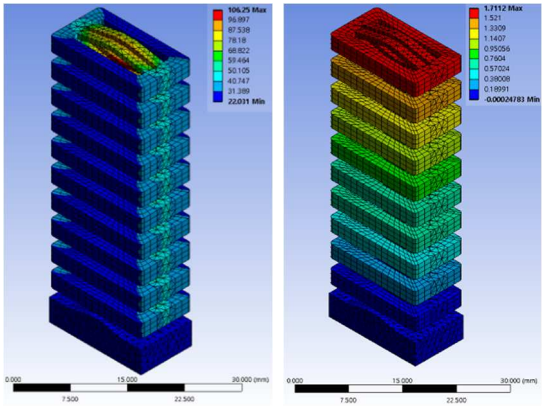

(a) (b)

Fig. 8 FEM analysis results: (a) temperature distribution and (b) retraction displacement at 6V

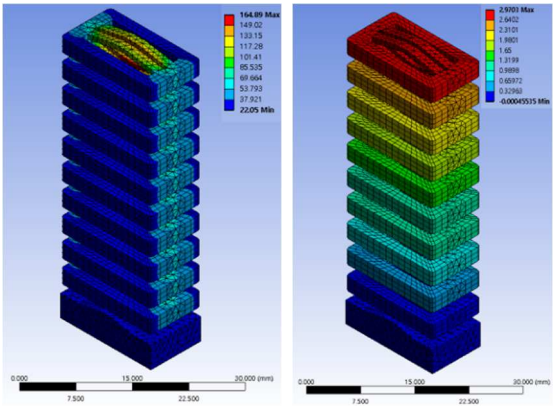

Fig. 9 FEM analysis results: (a) temperature distribution and (b) retraction displacement at 8V

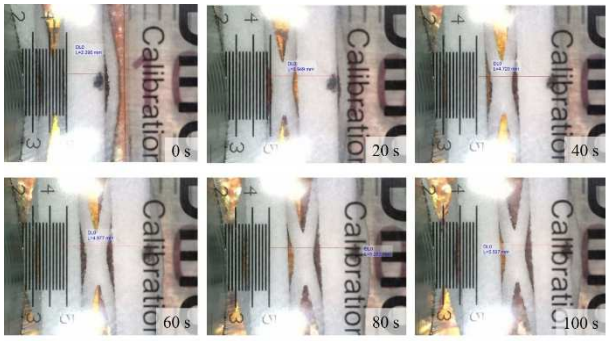

Fig. 10 Time lapse images for retraction motion of ExACT at 8V

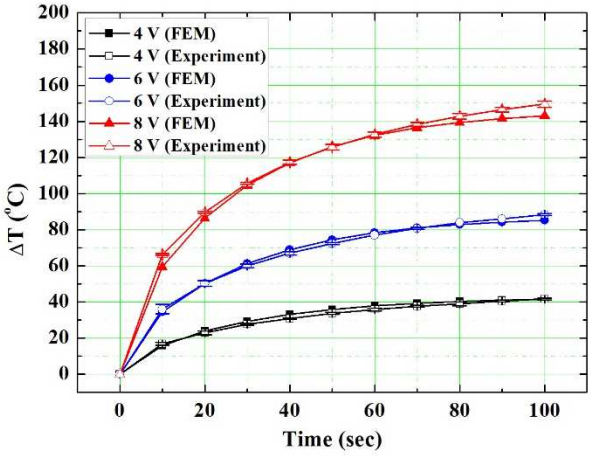

Fig. 11 Comparison of internal temperatures obtained with experiment and FEM analysis

was used as the material. ExACT is operated by inserting thin film heaters into the slots and electrically heating them. Figure 5 shows the fabricated ExACT, which was fabricated according to the intended design, despite its complexity.

In particular, the actuator proposed in this study has the advantage that it can be fabricated at a considerably low cost compared to actuators that use expensive materials such as piezoelectric materials.

The schematic of the setup for performance evaluation of ExACT is presented in Fig. 6. As shown in the lower left panel of Fig. 6, two thin film heaters were inserted into the inner slot of ExACT, and a thin film thermocouple was installed between the heaters to record the temperature. A general thin film heater (K05711980-A, WATLOW) composed of polyimide film with a metal resistor was used. The support structure of ExACT was attached to the base plate using polyimide tape, and the opposite end was designed as a moving end.

After successively supplying a voltage of 4, 6, and 8 V to the heater using a power supply (OPE-303QI, ODA), the change

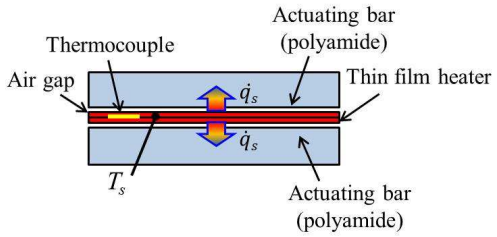

Fig. 12 Schematic cross section of ExACT where the heaters and thermocouple are loaded

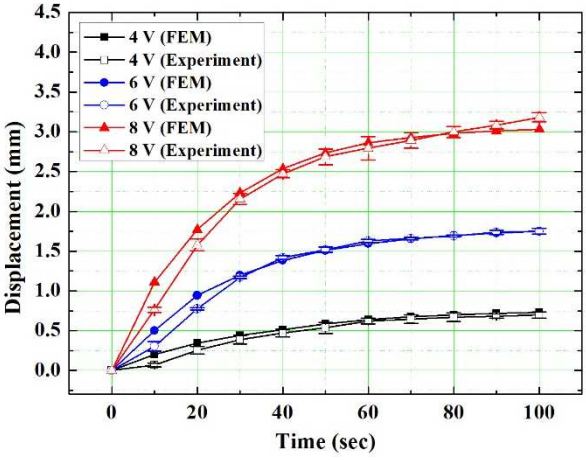

Fig. 13 Retraction displacement of ExACT as a function of time

in the length of the moving end (Δh) was measured using a charge-coupled device (CCD) microscope (AM7013MZT, Dino) for 100 seconds at 10 second intervals. At this time, as shown in the lower right panel of Fig. 6, the photographs of the length change were taken with a precision ruler in each photo and $\triangle h$ was precisely measured using image processing software.

5. Results and Discussion

Figures 7, 8, and 9 show the results of FEM analysis of temperature distribution and displacement of ExACT after 100 seconds at input voltages of 4, 6, and 8 V, respectively. the temperature distributions show that the temperature of the internal chevron DAS increased after 100 seconds, but the temperature of the external support bar showed little increase. This confirms that the thermal insulation design of ExACT was properly implemented, and it was possible to predict that the length of the support bar would remain unaffected by heat. Furthermore, by examining the extended displacement, the increase with respect to temperature can be confirmed. Figure 9 shows that the moving end of ExACT is extended up to 2.97

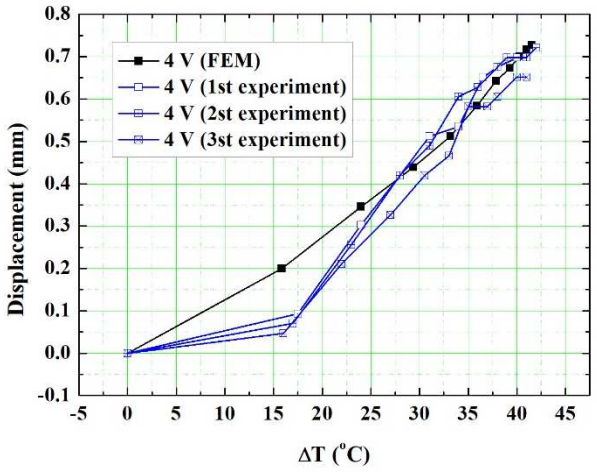

(a)

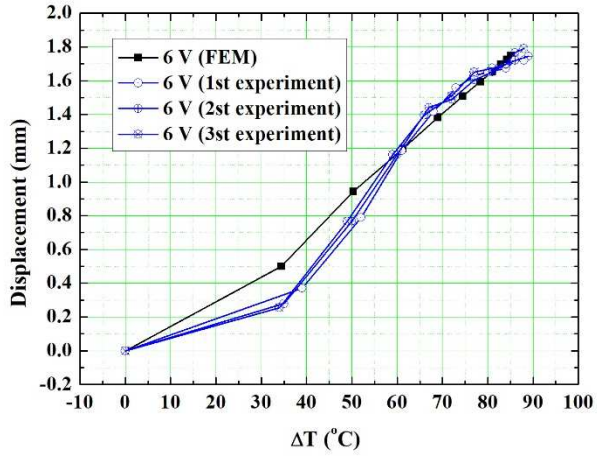

(b)

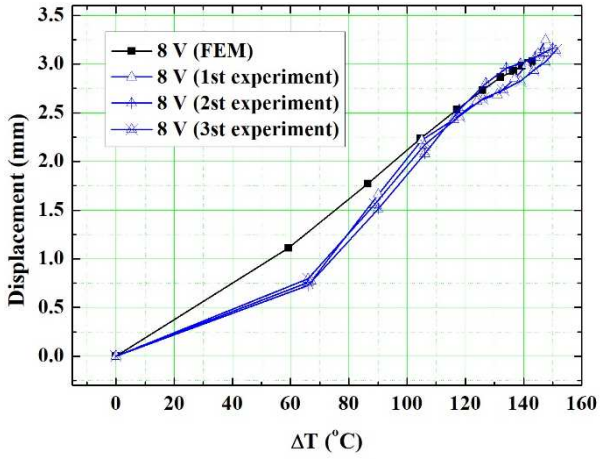

(c)

Fig. 14 Displacement of ExACT as a function of temperature at excitation voltages of (a) 4V, (b) 6V, and (c) 8V

mm when heated for 100 seconds at an input voltage of 8 V.

In Fig. 10, the time lapse images taken at one end of

ExACT at 20 second intervals using a CCD f microscope at an input voltage of 8 V are presented. Similar to the results obtained from the FEM analysis, it can be seen that the moving end of ExACT is extended on heating. The extended displacement of the end of ExACT was measured from the images including the precision ruler using image processing software.

Figure 11 presents a graphical comparison of the hourly temperature values obtained by measurements using a thermocouple mounted between two thin film heaters at input voltages of 4, 6, and 8 V and those obtained by FEM analysis. The temperature was measured thrice, and the mean and standard deviation of the measurement values were calculated, which are presented in Fig. 11. Since the resistance of the thin film heater is approximately 40 Ω, at input voltages of 4, 6, and 8 V, the power supplied to the heater is 0.40, 0.90, and 1.6 W, respectively. Figure 11 shows that the temperature increases in proportion to the power supplied to the heater. Thus, for 0.40 W (4 V) of power, the temperatures measured by the thermocouple after 40, 70, and 100 seconds were 30.8°C, 37.7°C, and 41.7 °C, respectively. For 0.90 W (6 V), the corresponding temperatures were 67.0°C, 80.7°C, and 88.3 °C, respectively. For 1.6 W (8 V), the recorded temperatures were 117.3°C, 138.3°C, and 149.5 °C, respectively. In addition, the internal temperature increased exponentially with heating time. ExACT has a structure with two heaters inserted between DAS made of polyamide as shown in Fig. 12. A thermocouple for measuring the temperature was placed between the two heaters. In general, the heat flux and time-dependent surface temperature in semi-infinite structures can be calculated using Eq. 8 as below.

$$T_S = T_i + \frac{\dot{q}_s}{k}\sqrt{\frac{4\alpha\tau}{\pi}} \tag{8}$$

In Eq. 8, T_s, and T_i denote the temperature of the heater surface and the initial temperature, respectively. The notations $\dot{q}_s$, k, α, and τ indicate the heat flux generated by the heater, the thermal conductivity of the bar used for measurement, the thermal diffusivity, and the time, respectively. Equation 8, shows that the temperature T_s of the heater surface is proportional to the heat flux, and increases exponentially with time τ. These characteristics can also be confirmed from the FEM analysis results shown in Fig. 11.

Figure 13 presents a graphical comparison of the extended displacement at the moving end of ExACT measured through experiments at each input voltage and that calculated through FEM analysis. The figure shows that the actuation displacement changes varies exponentially, similar to the temperature variation with time (Fig. 11).

In the case of the values of extended displacement with time shown in Fig. 13, the results of FEM analysis and experimental results were mostly similar, but in a section with a short heating time, the two sets of the results differed, which is attributed to the thermal energy required to heat the polyimide film constituting the heater during power supply. In addition, in the FEM analysis, the simulation was performed assuming that the heat flux corresponding to the supply power is directly applied to the surface of the slot where the heater is installed. However, in the actual experiments, a gap exists between the thin film heater and the slot, leading to the formation of a heat resistance layer between the heater and the bar. Owing to the heat resistance layer, the temperature of the DAS is lower than that in the FEM analysis. In particular, for short heating times or small supply voltages, the effect of the heat resistance layer is greater than that of the heat flux generated by the heater, which is assumed to result in the considerable difference between the FEM analysis results and the experimental results.

This phenomenon can also be observed in Figs. 12, 13, and 14. On average, the low temperature section, exhibited experimental values smaller than the FEM analysis values, which is attributed to the heat resistance layer between the heater and the operating bar. In addition, is deviations in the experimental environment such as ambient temperature and humidity are considered as a further cause of this difference.

Figure 14 shows that ExACT has a maximum actuation displacement of approximately 3.2 mm, which corresponds to about 21.1% of the height of the displacement amplification mechanism of 15.2 mm (number of unit actuators × $2h$), and about 7.6% of the total height of the actuator 42.0mm (number of unit actuators × H). Furthermore, instead of the materials used in existing artificial muscle-type actuators for micro air vehicles (MAVs), i.e., SMA and piezoelectric ceramic, SMP and EAP were used in this study. SMA has a strain value of approximately 8%; piezoelectric ceramic has a value of 0.1%, and SMP and EAP have a value of 50% or above [1]. Accordingly, it can be seen that the actuator developed in this study has a larger strain value than that of SMA and piezoelectric ceramic actuators.

6. Conclusion

In this study, we proposed a design of a novel ExACT based on the chevron actuator, which generates axial displacement 30 times greater than simple thermal displacement by heating the thin film heaters inserted into the inner slot. The chevron actuator comprises a V-shaped beam structure with limited lateral deformation, so the length of thermal expansion in axial direction is amplified. In particular, by applying a diamond-shaped displacement amplification mechanism with the chevron structure oriented axially, a high-displacement actuator with the length extending up to 20% of the initial length was implemented. The developed ExACT has a considerably complex shape with 10 unit actuators comprising a DAS of the same material and a support bar restricting the

lateral thermal displacement connected in series. The actuator is heated electrically using the thin film heaters inserted into an inner slot. Thus, the proposed actuator has the characteristics of an artificial muscle type actuator with axial displacement achieved by applying heat.

To fabricate the proposed ExACT with a highly complex structure, an SLS-type 3D printer was used. Polyamide, which has a high coefficient of thermal expansion and high operating temperature compared to other polymer-based materials was used for this purpose.

The natural convective heat transfer coefficient was calculated according to temperature. Based on those values, FEM analysis was performed to calculate the internal temperature distribution of the actuator, using twhich, thermo-mechanical analysis was performed to obtain the actuation displacement for different input voltages and temperatures in the transient section.

Voltages of 4,6, and 8V were successively supplied to the heater, and the change in the length of the end (Δh) was measured for 100 seconds at 10 second intervals using a CCD microscope and image processing software. A comparison of the experimental data with the FEM analysis result showed that the two sets of results were similar in terms of the heater temperature.

However, the FEM results of extended displacement with respect to temperature showed larger values than the experimental result, in the low temperature region; results in the high temperature region were similar. In the low temperature region, the difference between the experimental and FEM results is attributed to the heat resistance layer formed between the heater and the bar in operation. It is presumed that with increasing temperature, the effect from the heat resistance layer becomes smaller than the heat flux from the heater, leading to more similarities between the FEM and experimental results.

The thermoelastic actuator proposed in this study has the merit of large actuation displacement but also the drawback of a long operating time. In future research for applications in MAVs, we aim to conduct further research on the optimal design of the operating bar to shorten the operating time and a new operating mechanism to increase the actuation displacement.

Acknowledgments

This research was conducted with the support of the National Research Foundation of Korea (NRF-2019R1F1A1060772) funded by the government (Ministry of Science and ICT) in 2021.

References

[1] J. Sun, Q. Guan, Y. Liu, and J. Leng, “Morphing aircraft based on smart materials and structures: A state-of-the-art review,” *J. Intell. Mater. Syst. Struct.*, vol. 27, no. 17, pp. 2289–2312, 2016, doi: 10.1177/1045389X16629569.

[2] L. D. Peel, J. Mejia, B. Narvaez, K. Thompson, and M. Lingala, “Development of a simple morphing wing using elastomeric composites as skins and actuators,” *J. Mech. Des. Trans. ASME*, vol. 131, no. 9, pp. 0910031–0910038, 2009, doi: 10.1115/1.3159043.

[3] A. Fortini, A. Suman, M. Merlin, and G. L. Garagnani, “Morphing blades with embedded SMA strips: An experimental investigation,” *Mater. Des.*, vol. 85, pp. 785–795, 2015, doi: 10.1016/j.matdes.2015.07.175.

[4] C. S. Haines et al., “Artificial muscles from fishing line and sewing thread,” *Science*, vol. 343, no. 6173, pp. 868–872, 2014, doi: 10.1126/science.1246906.

[5] A. Potekhina and C. Wang, “Review of electrothermal actuators and applications,” *Actuators*, vol. 8, no. 4, 2019, doi: 10.3390/ACT8040069.

[6] H. Guckel, J. Klein, T. Christenson, K. Skrobis, M. Laudon, and E. G. Lovell, “Thermo-magnetic metal flexure actuators,” in *Technical Digest IEEE Solid-State Sensor and Actuator Workshop*, 1992, pp. 73–75, doi: 10.1109/SOLSEN.1992.228273.

[7] K. Alblalaihid, J. Overton, S. Lawes, and P. Kinnell, “A 3D-printed polymer micro-gripper with self-defined electrical tracks and thermal actuator,” *J. Micromechanics Microengineering*, vol. 27, no. 4, 2017, doi: 10.1088/1361-6439/aa631e.

[8] A. Sanjay Joshi, H. Mohammed, and S. M. Kulkarni, “Analysis of a Chevron Beam Thermal Actuator,” *IOP Conf. Ser. Mater. Sci. Eng.*, vol. 310, no. 1, 2018, doi: 10.1088/1757-899X/310/1/012123.

[9] X. J. Mu et al., “A compact circumferential scanned endoscopic imaging probe using a MEMS-driven pyramidal polygon reflector,” *Proc. IEEE Int. Conf. Micro Electro Mech. Syst.*, vol. 20, no. 6, pp. 902–905, 2012, doi: 10.1109/MEMSYS.2012.6170331.

[10] X. Zhang, B. Li, X. Li, and H. Xie, “A robust, fast electrothermal micromirror with symmetric bimorph actuators made of copper/tungsten,” 2015 *Transducers - 2015 18th Int. Conf. Solid-State Sensors, Actuators Microsystems*, pp. 912–915, 2015.

[11] S. Timoshenko, “Analysis of Bi-Metal Thermostats,” *J. Opt. Soc. Am.*, vol. 11, no. 3, pp. 233–255, 1925, doi: 10.1364/JOSA.11.000233.

[12] S. Kim, W. Kim, and Y. Kim, “Design and performance evaluation of thin-film actuators based on flexible Ni-Co substrates,” *Micro Nano Syst. Lett.*, vol. 8, no. 1, 2020, doi: 10.1186/s40486-020-00122-z.

[13] R. Cragun, L. L. Howell, and A. S. of M. Engineers,

"Linear Thermomechanical Microactuators," in Symposium, Micro-electro-mechanical systems; (MEMS) -1999-, vol. 1, pp. 181–188, [Online]. Available: https://www.tib.eu/de/suchen/id/BLCP%3ACN033314656.

[14] L. Que, J. S. Park, and Y. B. Gianchandani, "Bent-beam electrothermal actuators-Part I: Single beam and cascaded devices," *J. Microelectromechanical Syst*., vol. 10, no. 2, pp. 247–254, 2001, doi: 10.1109/84.925771.

[15] M. J. Sinclair, "A high force low area MEMS thermal actuator," in ITHERM 2000. *The Seventh Intersociety Conference on Thermal and Thermomechanical Phenomena in Electronic Systems* (Cat. No.00CH37069), 2000, vol. 1, pp. 127–132, doi: 10.1109/ITHERM.2000.866818.

[16] L. Segal, "The thermal expansion of reinforced nylon-6 composites through the matrix glass transition temperature," *Polym. Eng. Sci.*, vol. 19, no. 5, pp. 365–372, Apr. 1979, doi: https://doi.org/10.1002/pen.760190508.

[17] Y. Cengel and A. Ghajar, Heat and mass transfer: fundamentals and applications, 5th ed. McGraw-Hill Higher Education, 2014.